Influence of sorption on sound propagation in granular activated carbon[a]

R. Venegas & O. Umnova

Rodolfo Venegas[b]

Carbon Air Ltd, The Innovation Forum, 51 Frederick Road, Salford, England, M6 6FP and Acoustics Research Centre, University of Salford, Salford, England, M5 4WT

r.venegas@carbonair.eu

Olga Umnova

Acoustics Research Centre, University of Salford, Salford, England, M5 4WT

Olga.Umnova@salford.ac.uk

---

[b] Corresponding author. Now at Université de Lyon, Ecole Nationale des Travaux Publics de l'Etat, LGCB, Rue Maurice Audin, 69518 Vaulx-en-Velin Cedex, France

Granular activated carbon has numerous applications due to its ability to adsorb and desorb gas molecules. Recently, it has been shown to exhibit unusually high low frequency sound absorption [Venegas & Umnova, J. Acoust. Soc. Am., 130(5), 2765-2776, 2011] and [Bechwati et al, J. Acoust. Soc. Am., 132(1), 239-248, 2012]. This behavior is determined by both the multi-scale nature of the material, i.e. the existence of three scales of heterogeneities, and physical processes specific to micro- and nanometer-size pores, i.e. rarefaction and sorption effects. To account for these processes a model for sound propagation in granular activated carbon is developed in this work. A methodology for characterizing granular activated carbon which includes optical granulometry, flow resistivity measurements, and the derivation of the inner-particle model parameters from acoustical and non-acoustical measurements is also presented. The model agrees with measurements of normal incidence surface impedance and sound absorption coefficient on three different granular activated carbon samples.

Influence of sorption on sound propagation in granular activated carbon

R. Venegas & O. Umnova

Rodolfo Venegas

Carbon Air Ltd., The Innovation Forum, 51 Frederick Road, Salford, England, M6 6FP and Acoustics Research Centre, University of Salford, Salford, England, M5 4WT

r.venegas@carbonair.eu

Olga Umnova

Acoustics Research Centre, University of Salford, Salford, England, M5 4WT

Olga.Umnova@salford.ac.uk

I. INTRODUCTION

Activated carbon is manufactured by carbonizing raw material (e.g. coal, peat, wood, nut-shells, etc.) followed by an activation process[1,2]. The carbonisation is performed in an inert atmosphere at 700-1000C. The activation usually consists of selective gasification of individual carbon atoms conducted by reaction of the carbon with oxidising gases such as carbon dioxide or steam, or mixtures of these two gases (usually at 800-900 C). The combination of carbonization and activation creates a large surface area characterized by a hierarchical porosity ranging from nanometer to micrometer size pores within the material. Granular activated carbons consist of

highly porous particles with size usually close to 1 mm. It possesses pores ranging in size from nearly a millimetre to a nanometer, i.e. it has multiple scales of heterogeneities. Its large surface area determines its remarkable sorption characteristics. Sorption is a general term which refers to adsorption, desorption, and absorption (penetration of the fluid into the solid phase). The former is a physical or chemical process in which the fluid molecules are adhered on to a surface. Adsorption can also be understood as an increase in the fluid density in the vicinity of a fluid-solid interface. Desorption is the opposite phenomenon, i.e. the fluid molecules are released from the surface. The adherence in physical adsorption is caused by weak van der Waals forces while the chemical bonding is responsible for chemical adsorption. The release of the molecules is caused by either an increase of temperature or a decrease in pressure which results in a break of the weak physical bond[1,2].

The exploration of acoustical applications of granular activated carbon began after it was suggested that this material can increase the compliance of a loudspeaker enclosure[3]. The phenomenon was attributed to sorption processes that occur in the very small pores within the grains[3,4]. A similar behaviour has been observed in Helmholtz resonators fully and partially filled with granular activated carbon[5,6]. In addition, granular activated carbon has shown unusually large low frequency sound absorption[5,6,7], which has been attributed (at least partially) to sorption processes.

The effect of sorption on sound attenuation in straight cylindrical pores has been studied in Ref.[8] where the sorption dynamics was approximated by a Langmuir isotherm model. Mellow et al.[4] extended this work to account for rarefactions effects, which occur in pores with size l comparable to the mean free molecular path[9] $l_{mean} = \eta p^{-1} \sqrt{\pi R_g T / 2}$. The latter can be interpreted as the average distance travelled

by a molecule between two successive collisions[9], and depends on the dynamic viscosity η, the specific gas constant R_g, the gas pressure p, and the absolute gas temperature T. The ratio between these lengths $\mathrm{Kn} = l^{-1} l_{mean}$ is known as the Knudsen number[9], and measures the degree of rarefaction. Its value is used for assessing the validity of the continuum hypothesis. For $\mathrm{Kn} < 0.01$ the continuum hypothesis remains valid and the macroscopic acoustic description presented in Ref.[10,11,12] holds. For $0.01 < \mathrm{Kn} < 0.1$ (commonly referred to as the slip-flow regime) the effects due to the molecular nature of the gas start becoming considerable. The continuum description, however, is valid everywhere in the fluid except in a thin Knudsen layer close to the walls. In this layer even an approximate thermodynamic equilibrium is failed to be established due to an insufficient number of collisions between the gas molecules and the pore walls. To account for this, the continuum description is modified by allowing a degree of tangential-velocity slip[9,13]. The rarefaction effects are even stronger for $0.1 < \mathrm{Kn} < 10$ and a transition from slip- to free molecular flow is observed[9]. In this regime the fluid transport is mainly determined by a combination of Knudsen and binary diffusions[2,14,15,16]. The free flow regime is attained when $\mathrm{Kn} > 10$ and is characterised by negligible inter-molecular collisions[9] hence Knudsen diffusion is the dominating transport mechanism[2,16].

In the presence of sorption smaller pores are likely to be gradually filled with adsorbed gas molecules as the equilibrium pressure increases[15]. Depending on whether this quantity is smaller or larger than the capillary condensation pressure a combination of surface diffusion (i.e. mobility of the adsorbed molecules below monolayer coverage) and film condensate or capillary condensate flow would be the dominant transport mechanisms[15]. In pores with size comparable to the molecular size, the molecules are trapped within the force field of the pore walls and the

dominant transport mechanism is an activated diffusion process[2,17]. Similarly, molecular effects influence the thermal behaviour of materials with small characteristic pore size in the different regimes characterised by the Knudsen number[9]. For $0.01 < \mathrm{Kn} < 0.1$ the continuum description is modified to account for the temperature-jump on the pore boundaries using a boundary condition that states that the temperature is proportional to the normal component of the temperature gradient[9,18]. For even smaller pores the thermal behaviour might be better described using either higher-order temperature-jump boundary conditions or kinetic molecular models[9]. The influence of rarefaction effects on the acoustical properties of porous materials has been studied in Ref.[19,20].

Recently, the influence of sorption and diffusion on sound propagation in slit-like pores has been theoretically studied in Ref.[21]. This model and those described in the previous publications[4,8] are not directly applicable to granular activated carbon because i) they do not account for its multi-scale nature nor its geometry, and ii) their range of validity has not been assessed using the theory of homogenisation for periodic media (HPM)[12,22].

The predictions of the acoustical properties of granular activated carbon were made in Ref.[7] assuming that the material possesses three characteristic scales (double porosity material). However, this model did not include sorption and rarefaction effects at any scale. Hence, it was unable to accurately predict the acoustical properties of granular activated carbon at low frequencies. The reason for this is that the normalized static bulk modulus of granular activated carbon attains a value smaller than one[6,7], while the current theory of acoustics of porous media predicts its value to be the inverse of porosity (hence a value larger than one). Venegas and Umnova[7] suggested that the discrepancies may be explained by adding an additional scale to the introduced double

porosity model and including sorption processes that modify the bulk modulus of granular activated carbons into the modelling.

This idea is developed in the current work where a model for sound propagation in granular activated carbon and a methodology for its characterisation are presented. The model is introduced by making successive use of the theory of acoustics of multi-scale porous media derived using the method of homogenization for periodic media (HPM)[12,22]. It accounts for both the multi-scale nature of granular activated carbon and physical processes specific to small pores. The paper is organized as follows. In Section II.A the wave equation for single porosity materials including sorption and rarefaction effects is derived using HPM. A model for sound propagation in double porosity granular media[7] is then re-called in Section II.B. This model is generalised in Section II.C to account for a third porosity scale, i.e. granular activated carbon is modelled as a triple porosity material). Three characteristic pore sizes account for the existence of inter-granular pores and for two characteristic sizes of intra-granular pores. The results of Section II.A are used to model sound propagation at the intra-particle scales where the effects of rarefaction and sorption are significant. A methodology for the characterisation of granular activated carbon is presented in Section III.A. A comparison between the model predictions and measurements of surface impedance and sound absorption coefficient on three different samples of granular activated carbon with different microstructure is shown in section III.B. The main findings are summarized in Sec. IV.

II. THEORY

A. Sound propagation in single porosity materials accounting for processes specific to small pores

In this section the wave equation in single porosity materials including rarefaction and sorption effects is derived first. This is done by using the homogenisation technique for periodic media (HPM)[12,22]. The different transport mechanisms associated with the smallest pores are then discussed and included into the formulation.

Consider a periodic rigid-frame porous material that is saturated by air and supports sorption. Figure 1 shows a diagram with the two scales of the material.
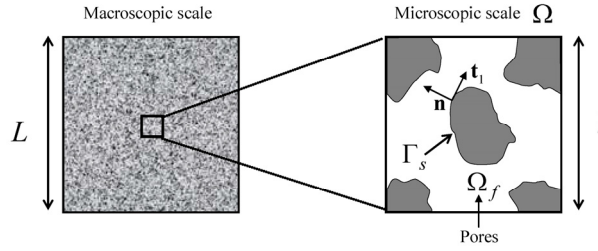

Figure 1 Diagram of the scales of a single porosity material supporting rarefaction and sorption effects (adapted from Ref.[12])

The macroscopic characteristic length is denoted as L (and is related to the sound wavelength λ as $L = |\lambda| / 2\pi$), and the microscopic characteristic length (or the period of the microstructure) as l. The latter is assumed to be comparable to the molecular mean free path l_{mean}. The material porosity is defined as $\phi = \Omega_f / \Omega$, where Ω_f is the open voids/pore volume and Ω is the volume of the representative elementary volume (REV). The disparity in length scales provides a small expansion parameter $\varepsilon = l / L \ll 1$ that ensures the existence of the REV. In addition, ε is

assumed to be much smaller than the Knudsen number, i.e. $\varepsilon \ll \mathrm{Kn} \ll 1$. The response of a single porosity sorptive material to a sound wave is described by the linearized equations of conservation of momentum [Eq. (1)], mass [Eq. (2)], energy [Eq. (3)], and by the equation of state [Eq. (4)], along with the slip and temperature-jump boundary conditions on the pore walls [Eqs. (5) and (6)].

$$\eta \nabla^2 \mathbf{u} - \nabla p = j\omega \rho_0 \mathbf{u}, \tag{1}$$

$$j\omega(\rho + \rho_a) + \rho_0 \nabla \cdot \mathbf{u} = 0, \tag{2}$$

$$\kappa \nabla^2 \tau + j\omega p = j\omega \rho_0 C_p \tau, \tag{3}$$

$$\frac{p}{P_0} = \frac{\tau}{\tau_0} + \frac{\rho}{\rho_0}, \tag{4}$$

$$\mathbf{u} = -c_v l_{mean} \left(\mathbf{t}_1 \cdot (\nabla \mathbf{u}) \cdot \mathbf{n} \right) \mathbf{t}_1 \text{ on } \Gamma_s, \tag{5}$$

$$\tau = c_t \frac{2\gamma}{(\gamma + 1)\mathrm{Pr}} l_{mean} (\nabla \tau \cdot \mathbf{n}) \text{ on } \Gamma_s. \tag{6}$$

Here ω is the angular frequency, C_p is the heat capacity at constant pressure, κ is the thermal conductivity, $\mathrm{Pr} = C_p \eta / \kappa$ is the Prandtl number, γ is the ratio between specific heats, and ρ_0, P_0, and τ_0 are the equilibrium pressure, density and temperature respectively. The oscillating velocity, pressure, density, temperature, and a density increment due to sorption are denoted as $\mathbf{u}$, p, ρ, τ, and ρ_a, respectively. Harmonic dependence of the type $e^{j\omega t}$ is assumed. The unit normal vector to the boundary Γ_s pointing outward from the pore region is denoted as $\mathbf{n}$ and the unit tangential vector collinear with the wall slip as $\mathbf{t}_1$. The parameters $c_v = (2 - \sigma_v) / \sigma_v$ and $c_t = (2 - \sigma_t) / \sigma_t$ are the velocity slip and temperature jump coefficients[9], which depend on the tangential σ_v and thermal σ_t accommodation

coefficients. In turn, these coefficients depend of the collision interaction laws between gas molecules and the pore walls (equal to 1 or 0 for fully diffuse or specularly reflective surfaces respectively), the nature of the saturating gas itself, its temperature, and pressure[9,19,23]. It is often assumed that $\sigma_v \approx \sigma_t = 1$, i.e. all the molecules are reflected diffusively[19,23].

The change in density due to sorption ρ_a is modelled using the Langmuir model[24,2]. This model relates the rate of adsorption and desorption and assumes that[24,2] : i) the surface of the solid is homogeneous, i.e. the adsorption energy is constant over all sites of the surface; ii) adsorption is localized, i.e. the molecules are adsorbed at definite localized sites; iii) each site can accommodate only one molecule, i.e. monolayer coverage; iv) the adsorbed molecules do not interact with each other. It is worth reminding that the pressure variations caused by a sound wave are very small. This means that the global nature of the isotherm is not of importance. Here the Langmuir model is adopted because of both it is widely known and to facilitate further comparisons between values of the sorption parameter of the model and those found in literature. The equation of the Langmuir model is given by:

$$\frac{d\tilde{\rho}_a}{dt} = k_a \tilde{p}\left(\rho_N - \tilde{\rho}_a\right) - k_d \tilde{\rho}_a \, . \tag{7}$$

Here $\tilde{\rho}_a = \rho_{a0} + \rho_a e^{j\omega t}$ and $\tilde{p} = P_0 + pe^{j\omega t}$. The term ρ_{a0} represents the equilibrium density of the adsorbed molecules. The maximum value of the density increment due to sorption is denoted as ρ_N while the adsorption and desorption constants as k_a (in Pa^{-1} s^{-1}) and k_d (in s^{-1}) respectively. In general, these depend on temperature and the pore size[2]. By assuming that $p \ll P_0$ and $\rho_a \ll \rho_{a0}$ Eq. (7) can be linearized to obtain:

$$\rho_a = \frac{k_a k_d \rho_N}{(j\omega + \omega_a)\omega_a} p, \tag{8}$$

where the sorption characteristic frequency ω_a is defined as:

$$\omega_a = k_a P_0 + k_d. \tag{9}$$

The estimates of the dimensionless numbers are now presented. The macroscopic characteristic length L is considered as a reference length (hence the subscript L in the dimensionless number estimates below). The procedure for determining the estimates of the dimensionless numbers, apart from that for those related to sorption effects, is well known and can be found, for example, in Ref.[12].

The ratio of the pressure gradient to the viscous forces per unit volume is given by $Q = |\nabla p| / |\eta \nabla^2 \mathbf{u}|$. Since the flow is forced by the macroscopic pressure gradient and occurs in the pores, it can be shown that $Q_L = O(\varepsilon^{-2})$. The transient Reynolds number $R_t = |j\omega\rho_0\mathbf{u}| / |\eta\nabla^2\mathbf{u}|$ is defined as the ratio of the transient and the viscous term in Eq. (1). Under acoustic excitation, the inertial term acts at the local scale, which means that $R_{tL} = O(\varepsilon^{-2})$. The Strouhal number S_t characterizes the transient behaviour of the flow and is given by $S_t = |j\omega\rho| / |\rho_0\nabla\cdot\mathbf{u}|$. A macroscopic transient behaviour corresponds to $S_{tL} = O(1)$. The dimensionless number that relates the change in density due to sorption and the spatial variations of fluid volume is given by $Z_t = |j\omega\rho_a| / |\rho_0\nabla\cdot\mathbf{u}|$. Considering that the variations of acoustic density are of the same order as the variations of the density increment due to sorption one can obtain the following estimate $Z_{tL} = O(1)$. The following dimensionless number $N_t = |j\omega\rho_0 C_p\tau| / |\kappa\nabla^2\tau|$ describes the ratio of the inertial and conductivity terms in the

equation of conservation of energy. The thermal exchanges occur at the pore scale and the conduction and transient terms are of the same order of magnitude, which yields $N_{tL} = O(\varepsilon^{-2})$. The dimensionless number relating the heat source due to pressure variations and the conduction term, $M_t = |j\omega p| / |\kappa \nabla^2 \tau|$, is estimated as $M_{tL} = O(\varepsilon^{-2})$ since the former is of the same order as the inertial term. Finally, the dimensionless numbers quantifying the influence of the slip and temperature-jump boundary conditions are given by[6,27] $B_v = |-c_v l_{mean} (\mathbf{t}_1 \cdot (\nabla \mathbf{u}) \cdot \mathbf{n}) \mathbf{t}_1| / |\mathbf{u}|$ and $B_t = |(c_t 2\gamma l_{mean} / (\gamma+1)\mathrm{Pr})(\nabla \tau \cdot \mathbf{n})| / |\tau|$. Noting that[23] $c_v = O(1)$ and $c_t = O(1)$, they are estimated as $B_{vL} = O(\varepsilon \mathrm{Kn})$ and $B_{tL} = O(\varepsilon \mathrm{Kn})$ respectively.

Now equations (1)-(6) can be written in dimensionless form as:

$$\varepsilon^2 \eta \nabla^2 \mathbf{u} - \nabla p = j\omega \rho_0 \mathbf{u}, \tag{10}$$

$$j\omega \left(\rho + \frac{k_a k_d \rho_N}{(j\omega + \omega_a)\omega_a} p \right) + \rho_0 \nabla \cdot \mathbf{u} = 0, \tag{11}$$

$$\varepsilon^2 \kappa \nabla^2 \tau + j\omega p = j\omega \rho_0 C_p \tau, \tag{12}$$

$$\frac{p}{P_0} = \frac{\tau}{\tau_0} + \frac{\rho}{\rho_0}, \tag{13}$$

$$\mathbf{u} = -\varepsilon \mathrm{Kn} (\mathbf{t}_1 \cdot (\nabla \mathbf{u}) \cdot \mathbf{n}) \mathbf{t}_1 \text{ on } \Gamma_s, \tag{14}$$

$$\tau = \varepsilon \frac{2\gamma \mathrm{Kn}}{(\gamma+1)\mathrm{Pr}} (\nabla \tau \cdot \mathbf{n}) \text{ on } \Gamma_s. \tag{15}$$

Here the spatial variables are defined as $y = \mathbf{X}/l$ and $x = \mathbf{X}/L$ with $\mathbf{X}$ being the physical space variable of the system and the macroscopic length L has been chosen as a reference. Hence the differential operators in Eqs. (10)-(15) take the form $\nabla = \nabla_x + \varepsilon^{-1} \nabla_y$ and $\nabla^2 = \Delta_x + 2\varepsilon^{-1} \nabla_{xy} + \varepsilon^{-2} \Delta_y$. The quantities are looked for in

the form of asymptotic expansions in powers of the small parameter ε as

$$\Xi(x,y) = \sum_{i=0}^{\infty} \varepsilon^i \Xi^{(i)}(x,y) \quad \text{where} \quad \Xi = p, \mathbf{u}, \rho, \rho_a, \tau, \mathbf{t}_1.$$ These are now substituted into

Eqs. (10)-(15) and the terms of the same order are identified. At ε^{-1}, it follows from

the equation of momentum conservation that $\nabla_y p^{(0)} = 0$, which means that the

pressure depends only on the macroscopic spatial variable, i.e. $p^{(0)} = p^{(0)}(x)$.

Subsequent orders of expansion provide the following set of equations:

$$\eta \Delta_y \mathbf{u}^{(0)} - \nabla_y p^{(1)} - \nabla_x p^{(0)} = j\omega\rho_0 \mathbf{u}^{(0)}, \tag{16}$$

$$\nabla_y \cdot \mathbf{u}^{(0)} = 0, \tag{17}$$

$$\mathbf{u}^{(0)} = -\text{Kn}\left(\mathbf{t}_1^{(0)} \cdot \nabla_y \mathbf{u}^{(0)} \cdot \mathbf{n}\right)\mathbf{t}_1^{(0)} \quad \text{on } \Gamma_s, \tag{18}$$

$$\kappa \Delta_y \tau^{(0)} + j\omega p^{(0)} = j\omega\rho_0 C_p \tau^{(0)}, \tag{19}$$

$$\tau^{(0)} = \frac{2\gamma \text{Kn}}{(\gamma+1)\text{Pr}} \nabla_y \tau^{(0)} \cdot \mathbf{n} \quad \text{on } \Gamma_s, \tag{20}$$

$$\frac{p^{(0)}}{P_0} = \frac{\tau^{(0)}}{\tau_0} + \frac{\rho^{(0)}}{\rho_0}, \tag{21}$$

$$j\omega\left(\rho^{(0)} + \frac{k_a k_d \rho_N}{(j\omega + \omega_a)\omega_a} p^{(0)}\right) + \rho_0\left(\nabla_x \cdot \mathbf{u}^{(0)} + \nabla_y \cdot \mathbf{u}^{(1)}\right) = 0. \tag{22}$$

The oscillatory Stokes [Eqs. (16)-(18)] and heat conduction problems [Eqs. (19)-(20)]

are decoupled and both constitute sets of linear equations. They may therefore be

formally expressed as linear operators acting on the source terms, i.e.

$$\mathbf{u}^{(0)} = -\frac{\hat{\mathbf{k}}(y,\omega,\text{Kn})}{\eta} \cdot \nabla_x p^{(0)}, \tag{23}$$

$$p^{(1)} = -\hat{\boldsymbol{\pi}}(y,\omega,\text{Kn}) \cdot \nabla_x p^{(0)} + \hat{p}^{(1)}, \tag{24}$$

$$\tau^{(0)} = \frac{\widehat{k'}(y, \omega, \text{Kn})}{\kappa} j\omega p^{(0)}. \tag{25}$$

Here $\widehat{\mathbf{k}}(y, \omega, \text{Kn})$ and $\widehat{k'}(y, \omega, \text{Kn})$ denote the $\Omega -$ periodic microscopic dynamic viscous permeability tensor and the microscopic dynamic thermal permeability distribution respectively. Note that the pressure field has been expressed in terms of zero mean $\widehat{\boldsymbol{\pi}}$ part and an integration constant $\widehat{p}^{(1)}$.

Substituting Eqs. (23)-(25) into Eqs. (16)-(20), two decoupled boundary value problems are formulated:

$$j\omega \frac{\rho_0}{\eta} \widehat{\mathbf{k}} - \Delta_y \widehat{\mathbf{k}} + \nabla_y \widehat{\boldsymbol{\pi}} = \mathbf{I}, \tag{26}$$

$$\nabla_y \cdot \widehat{\mathbf{k}} = 0, \tag{27}$$

$$\widehat{\mathbf{k}} = -\text{Kn}\left(\mathbf{t}_1^{(0)} \cdot \nabla_y \widehat{\mathbf{k}} \cdot \mathbf{n}\right) \mathbf{t}_1^{(0)} \text{ on } \Gamma_s. \tag{28}$$

$$j\omega \frac{\rho_0 C_p}{\kappa} \widehat{k'} - \Delta_y \widehat{k'} = 1, \tag{29}$$

$$\widehat{k'} = \frac{2\gamma \text{Kn}}{(\gamma + 1)\text{Pr}} \nabla_y \widehat{k'} \cdot \mathbf{n} \text{ on } \Gamma_s, \tag{30}$$

where $\mathbf{I}$ is the unitary second-rank tensor. The dynamic permeabilities are then calculated by averaging the solution over the REV as:

$$\mathbf{k}(\omega, \text{Kn}) = \left\langle \widehat{\mathbf{k}}(y, \omega, \text{Kn}) \right\rangle_y, \tag{31}$$

$$k'(\omega, \text{Kn}) = \left\langle \widehat{k'}(y, \omega, \text{Kn}) \right\rangle_y. \tag{32}$$

The average is taken over the complete volume, i.e.

$$\langle \bullet \rangle_y = \frac{1}{\Omega} \int_{\Omega_f} (\bullet) d\Omega. \tag{33}$$

The macroscopic description is then obtained by taking the volume average over the compatibility condition (Eq. (22)). Note that the equation of state has been used to express $\rho^{(0)}$ in this equation:

$$\left\langle j\omega\left(\frac{p^{(0)}}{P_0} - \frac{\tau^{(0)}}{\tau_0} + \frac{k_a k_d}{(j\omega+\omega_a)\omega_a}\frac{\rho_N}{\rho_0}p^{(0)}\right) + \nabla_x \cdot \mathbf{u}^{(0)} + \nabla_y \cdot \mathbf{u}^{(1)}\right\rangle_y = 0. \quad (34)$$

Using the divergence theorem and considering periodicity, the slip boundary condition, orthogonality, and the thermodynamic identity $P_0/\tau_0 = \rho_0 C_p(\gamma-1)/\gamma$, one can obtain the macroscopic wave equation for pressure:

$$\frac{j\omega p^{(0)}}{E(\omega,\mathrm{Kn},k_a,k_d)} = \nabla_x \cdot \left(\frac{\mathbf{k}(\omega,\mathrm{Kn})}{\eta}\nabla_x p^{(0)}\right). \quad (35)$$

It is clear that the overall (macroscopic) flow is not affected by sorption effects. The dynamic viscous permeability is given by Eq. (31) and does not depend on the sorption parameters. Its properties have been analysed, for example, in Ref.[12,27]. On the other hand, the dynamic bulk modulus is significantly altered by sorption and can be written in terms of the classical contribution to thermal dissipation due to heat conduction including rarefaction effects $E_h(\omega,\mathrm{Kn})$ and one additional contribution, $E_s(\omega,k_a,k_d)$, due to sorption processes, i.e.

$$E(\omega,\mathrm{Kn},k_a,k_d) = \left(E_h^{-1} + E_s^{-1}\right)^{-1}, \quad (36)$$

where

$$E_h(\omega,\mathrm{Kn}) = \frac{\gamma P_0}{\phi}\left(\gamma - j\omega\rho_0 C_p(\gamma-1)\frac{k'(\omega,\mathrm{Kn})}{\phi\kappa}\right)^{-1}. \quad (37)$$

$$E_s(\omega,k_a,k_d) = \frac{\gamma P_0}{\phi}\left(\frac{\gamma P_0 k_a k_d}{(j\omega+\omega_a)\omega_a}\frac{\rho_N}{\rho_0}\right)^{-1}. \quad (38)$$

This general formulation can be simplified as follows. For an isotropic material (or considering only a preferential flow direction) the viscous permeability becomes a scalar, i.e. $\mathbf{k} = k\mathbf{I}$. The viscous characteristic frequency, which determines the transition from viscous to inertia-dominated sound propagation in the material, is given by[10,11,12] $\omega_v = \eta\phi / \rho_0 \alpha_\infty k_0$, where α_∞ is the tortuosity and k_0 is the static viscous permeability. For materials with pore size in the order of the molecular mean free path $\omega_v \approx 1$ GHz at normal conditions[19]. Hence the sound propagation through the material can be assumed viscosity-dominated in the audible frequency range and the dynamic permeability in Eq. (35) can be approximated by its static value, i.e. $k(\omega \ll \omega_v, \mathrm{Kn}) = k_0(\mathrm{Kn})$. Since the thermal characteristic frequency is in the order[10,12] of the viscous characteristic frequency, i.e. $\omega_t = O(\omega_v)$, the sound propagation can be assumed isothermal and the dynamic bulk modulus associated to heat conduction (Eq. (37)) can be approximated by its isothermal value, i.e. $E_h(\omega \ll \omega_t) = P_0 / \phi$.

Furthermore, the adsorbed layer can be considered in equilibrium with the fluid phase since the average residence time of adsorption (i.e. the inverse of the sorption characteristic frequency) ranges from 10^{-13} to 10^{-9} s for physical adsorption[2]. Hence one can estimate the dynamic bulk modulus in the audible frequency range associated to sorption effects as $E_s(\omega \ll \omega_a) = P_0 / (\phi \rho_N \rho_0^{-1} \psi)$. Here the dimensionless parameter $\psi = P_0 b / (P_0 b + 1)^2$ depends on both the equilibrium pressure and the Langmuir constant $b = k_a / k_d$. The static bulk modulus is therefore given by:

$$E(\omega \to 0) = E_0 = \frac{P_0}{\phi} \frac{1}{\left(1 + \rho_N \rho_0^{-1} \psi\right)}. \tag{39}$$

This expression shows that the bulk modulus is modified by sorption effects if the term $\rho_N \rho_0^{-1} \psi$ is not negligible. Furthermore, its value normalized to the equilibrium pressure, i.e. E_0 / P_0, can be smaller than unity. For a porous material with circular cylindrical pores with pore radius r_n and porosity ϕ_n, the maximum value of the density increase associated to sorption is given by[4]:

$$\rho_N = \frac{2\phi m}{r_n S_m}, \tag{40}$$

where m is the mass of the saturating fluid molecule and S_m is the area occupied by each molecule. For air, these are given by $m = 4.8106 \cdot 10^{-26}$ kg and $S_m = 4\pi r_{air}^2 = 4.3265 \cdot 10^{-19}$ m^2, where the radius of an air molecule is[28] $r_{air} = 1.855 \cdot 10^{-10}$ m. Introducing this expression into Eq. (39) one concludes that the classical static bulk modulus is recovered when $\rho_N \rho_0^{-1} \to 0$ and/or $\psi \to 0$. The former occurs when the pores are large while the latter when either $P_0 b \to 0$ (i.e. $P_0 k_a \ll k_d$) or $P_0 b \to \infty$ (i.e. $P_0 k_a \gg k_d$).

As the effect of sorption on the bulk modulus is strong in the smaller pores (see Eq.(40)), the processes specific to them should be discussed. For pores smaller than the molecular mean free path the Knudsen number becomes large and the dominant transport mechanism is Knudsen diffusion[9,16] rather than viscous slip flow. It states that the diffusive transport is proportional to the pressure gradient[2,9,16,29] and the filtration velocity is given by:

$$\left\langle \mathbf{u}^{(0)} \right\rangle_y = -A \cdot \nabla_x p^{(0)}, \tag{41}$$

where $A = D_g / P_0$ and the Knudsen diffusion coefficient for an array of cylindrical pores is given by[2,29] $D_g = (\phi_n r_n / 3)\sqrt{8 R_g T / \pi}$. The macroscopic wave equation Eq.

(35), however, still remains valid, although with a modified "permeability", and can be obtained by replacing the argument of the divergence in Eq. (35) by $A \cdot \nabla_x p^{(0)}$.

When molecular diffusion is also present, the Knudsen diffusion coefficient in Eq. (41) should be replaced by an effective diffusion coefficient given by $D_e^{-1} = D_{ij}^{-1} + D_g^{-1}$, where D_{ij} is the binary gas diffusivity[2].

Even smaller pores are expected to be filled with adsorbed gas molecules at normal conditions and the fluid transport is primarily determined by capillary condensate flow[2,15], for which the filtration velocity is given by Eq. (41) and $A = k_{0n} / \eta_l$. Here η_l is the dynamic viscosity of the condensate and for the case of cylindrical pores[10] $k_{0n} = \phi_n r_n^2 / 8$.

In pores with size comparable to that of the saturating fluid molecules, the latter are trapped within the force field of the pore walls and the dominant transport mechanism is determined by an activated diffusion process showing an Arrhenius temperature dependence[2,17]. In this case, the filtration velocity is given by Eq. (41) with $A = D_c / P_0$, where the configurational diffusivity (also known as micropore or intracrystalline diffusivity) is denoted as $D_c = D_C c_f$. Here c_f is the thermodynamic correction factor, which equals to one in the Henry's or low coverage region, or for small differential changes in pressure or concentration[2]; and $D_C = D_{C\infty} \exp\left(-E_c / R_g \tau\right)$ is the corrected diffusivity. In this expression, $D_{C\infty}$ represents the corrected diffusivity at infinite temperature and E_c is the activation energy, which is usually one-third to one-half of the heat of adsorption[2,17]. It should be noted that a surface resistance at the nanopore mouth may be considered, but this would be in series with the mass transfer diffusion determined by the configurational

diffusivity[21]. Hence the surface resistance effect may be included into a lumped diffusivity without changing the general structure of the model.

All these transport processes are likely to be simultaneously occurring in the intra-granular pores of activated carbon, however their combined influence on the macroscopic flow is, as it will be shown in Section IIC, negligible compared to that of the mesoscopic (i.e. integranular) fluid network. Hence a detailed description of the fluid transport at the very small scales might not be required in a first approximation. It is worth noting that the expression derived for the bulk modulus (Eq. (39)) remains unaffected by the variety of possible diffusion mechanisms because it depends on the variation of density over pressure and not on the filtration velocity.

As has been shown in Ref.[8], the direct application of the model developed in this section to granular activated carbon does not accurately predict its acoustical properties. This is because this model, while accounting for sorption and rarefaction or diffusion effects, does not provide an adequate representation of both the geometry of the material and the several scales of heterogeneities of granular activated carbons. The double porosity model introduced in Ref.[7] takes both of these features into account but does not include sorption effects. This model is briefly recalled in the next section and will then be extended in Section III to include a third scale of heterogeneities and the effects specific to small pores. The latter will be done using the results derived above.

B. Sound propagation in double porosity granular materials

Three characteristic lengths can be identified in a double porosity granular material[7,26] (see Figure 2). The characteristic size l_p is determined by the size of the meso-

heterogenities, which for a granular porous material corresponds to the particle size. The characteristic size l_m is determined by the size of the pores within the particles and is comparable to l_{mean}. To model the material as an homogenous equivalent fluid the assumption of separation of scales should be satisfied, e.g. $\varepsilon = l_p / L \ll 1$ and $\varepsilon_0 = l_p / l_m \ll 1$. The meso and micro porosities are $\phi_p = \Omega_{fp} / \Omega_p$ and $\phi_m = \Omega_{fm} / \Omega_m$ respectively, where Ω_{fp} and Ω_{fm} are the open voids/pore volume, and Ω_p and Ω_m denote the volume of the REVs. The overall porosity of the material is given by $\phi_{db} = \phi_p + \left(1 - \phi_p\right)\phi_m$. The subscript *db* (meaning "double bulk modulus") denotes a double porosity quantity.
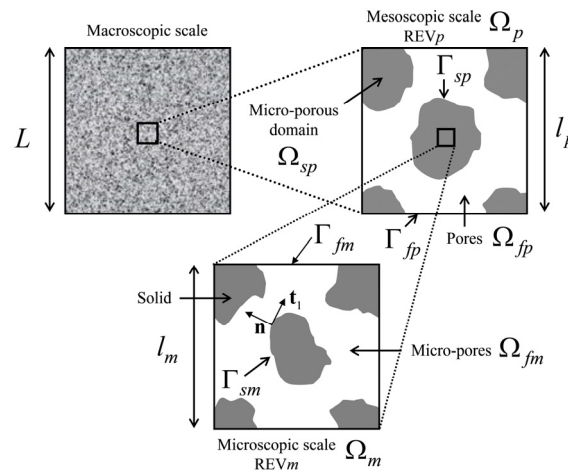

Figure 2: Diagram of the scales of a double porosity material (adapted from Ref.[26])

The wave equation in a rigid-frame double porosity granular material has the same general form[6,7,25,26,29] as that of Eq. (35). However, E and $\mathbf{k}$ should be replaced by the dynamic bulk modulus E_{db} and dynamic viscous permeability $\mathbf{k}_{db}$ of the double porosity granular material. The macroscopic acoustic behaviour is significantly affected by the interscale ratio ε_0. In the case of high-permeability contrast, i.e.

$\varepsilon_0 \approx 10^{-3}$, the pores in the particles have negligible contribution to the macroscopic fluid flow and the dynamic permeability $\mathbf{k}_{db}$ coincides with that of a packing of solid particles[6,7,26], i.e. $\mathbf{k}_{db}(\omega) = \mathbf{k}_p(\omega) + (1 - \phi_p) \mathbf{k}_m(\omega) \approx \mathbf{k}_p(\omega)$, where $\mathbf{k}_p$ and $\mathbf{k}_m$ are the dynamic permeability tensors of the mesoscopic and the microscopic domains. The dynamic bulk modulus is given by[6,7,26]:

$$E_{db}(\omega, \mathrm{Kn}) = \left(\frac{1}{E_p(\omega)} + \frac{(1 - \phi_p)}{E_m(\omega, \mathrm{Kn})} F_d \left(\omega \frac{P_0}{\phi_m E_m(\omega, \mathrm{Kn})} \right) \right)^{-1}, \qquad (42)$$

where F_d is a function that describes pressure diffusion effects, and E_p and E_m are the dynamic bulk modulus of the mesoscopic and microscopic domains, which can be calculated using Eq. (37). In the case of low-permeability contrast, i.e. $\varepsilon_0 \approx 10^{-1}$, the dynamic viscous permeability of the microscopic fluid network should be included in the calculation of the overall permeability and F_d should be replaced by 1 in Eq. (42) (see Ref.[6,7,26]).

This general formulation is now applied to model an unconsolidated double porosity granular material as an array of identical porous spheres[6,7]. The pores in the spheres are assumed cylindrical. The particle radius and the intergranular porosity are denoted as r_p and ϕ_p, while the micropore radius and microporosity as r_m and ϕ_m, respectively. The dynamic viscous and thermal permeabilities of the meso domain are calculated with models derived using a self-consistent approach[30,31]. In particular, the model for the dynamic viscous permeability considered here is the so-called P-estimate, which is given by[30,31]:

$$k_p(\omega) = \frac{-j\delta_v^2}{(1 - 3C/x^2)}, \qquad (43)$$

where

$$C = \frac{Ax + B\tanh\left(x\left(\beta - 1\right)\right)}{ax + b\tanh\left(x\left(\beta - 1\right)\right)}, \tag{44}$$

$$A = \left(3 + \left(\beta x\right)^2\right)\left(1 + \frac{x^2}{6}\right) - 3\beta\left(1 + \frac{x^2}{2}\right), \tag{45}$$

$$B = \left(3 + \left(\beta x\right)^2\right)\left(1 + \frac{x^2}{2}\right) - 3\beta x^2\left(1 + \frac{x^2}{6}\right), \tag{46}$$

$$a = \frac{1}{3}\left(3 + \left(\beta x\right)^2\right) - 3\beta - \frac{2}{\beta}\left(1 + \frac{x^2}{6}\right) + \frac{4}{\cosh\left(x(\beta - 1)\right)}, \tag{47}$$

$$b = 3 + \beta\left(\beta - 1\right)x^2 - \frac{2}{\beta}\left(1 + \frac{x^2}{2}\right), \tag{48}$$

$$\beta = \left(1 - \phi_p\right)^{1/3}, \ x = j^{1/2}r_p / \beta\delta_v, \text{ and } \delta_v = \sqrt{\eta / \rho_0\omega}. \tag{49}$$

The static viscous permeability is recovered from Eq. (43) assuming that frequency tends to zero[30].

$$k_{0p} = \left(\frac{r_p^2}{3\beta^2}\right)\left(\frac{\left(2 + 3\beta^5\right)}{\beta\left(3 + 2\beta^5\right)} - 1\right). \tag{50}$$

The dynamic thermal permeability is given by[31]:

$$k'_p(\omega) = -j\delta_t^2\left(1 - \beta^3 + \frac{3\beta}{x_t^2}\left(\beta x_t\frac{1 + x_t\tanh\left(x_t\left(\beta - 1\right)\right)}{x_t + \tanh\left(x_t\left(\beta - 1\right)\right)} - 1\right)\right), \tag{51}$$

where $x_t = x / \sqrt{\text{Pr}}$ and $\delta_t = \sqrt{\text{Pr}}\delta_v$

The dynamic viscous permeability k_m is calculated using[19] Eq. (52) and the bulk modulus E_m is calculated by setting $\phi = \phi_m$ and $k' = k'_m$ in Eq. (37) and considering that k'_m is given by[19] Eq. (53).

$$k_m(\omega, \text{Kn}) = -j\phi_m\delta_v^2\left(1 - G_c\left(s_c, \text{Kn}\right)\right). \tag{52}$$

$$k'_m(\omega, \text{Kn}) = -j\phi_m\delta_t^2\left(1 - G_c\left(\sqrt{N_{pr}}s_c, 2\gamma\text{Kn} / (\gamma + 1)\text{Pr}\right)\right), \tag{53}$$

$$G_c\left(s,\text{Kn}\right)=\frac{2}{s}\frac{J_1\left(s\right)}{J_0\left(s\right)-\text{Kn}sJ_1\left(s\right)}. \tag{54}$$

In these equations $s_c=j^{3/2}r_m/\delta_v$, $\text{Kn}=l_{mean}/r_m$, and $J_{0,1}$ are Bessel functions of the first kind of order 0 and 1.

Finally, the function that describes pressure diffusion effects, and the interscale coupling, is given by[7]:

$$F_d(z)=\frac{3}{z^2}\left(1-z\cot\left(z\right)\right),\text{ with }z=r_p\omega\sqrt{\eta/j\omega k_m E_m}. \tag{55}$$

C. A model for sound propagation in granular activated carbon

A complete model for sound propagation in granular activated carbon is introduced in this section. The model assumes that granular activated carbon features four scales (see Figure 3) and can be modelled as a collection of identical porous spheres in which the two inner-particle scales (e.g. microscopic scale and, in addition to it, a nanoscopic scale) are both modelled as arrays of cylindrical pores. The introduction of a nanoscopic scale is motivated by the well documented existence of nanopores in granular activated carbon[1]. Moreover, it was experimentally found[7] that absorption of low frequency sound by a granular activated carbon is in direct correlation with its nanopore volume: activated carbons with larger nanopore volume show a much improved low frequency sound absorption[7].

It is worth mentioning that pores with size smaller than 2 nm are called micropores in the IUPAC recommendation[32]. However, as argued in Ref.[2], this denomination is arbitrary. In order to keep our terminology compatible with earlier works on acoustics of multi-scale porous materials[6,7,25,26] and to provide a direct reference to the pore size, the pores at the nanoscopic scale are denoted as "nanopores", while those at the

microscopic scale are called "micropores". This means that what is called "nanopore volume" here is analogous to "micropore volume" as proposed in Ref.[32].
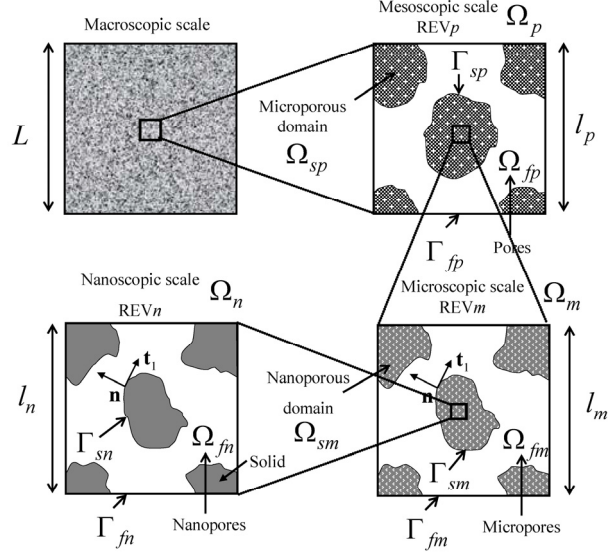

Figure 3: Diagram of the scales of a triple porosity sorptive material

The macroscopic scale is determined by the wavelength in the material while the mesoscopic, microscopic, and nanoscopic scales are characterized by their characteristic lengths, i.e. l_p, l_m, and l_n. These scales have porosities ϕ_p, ϕ_m, and ϕ_n, which are the meso, micro, and nano porosities respectively. Note that the subscript *tb* (meaning "triple bulk modulus") indicates a triple porosity quantity. The overall porosity of the material is given by:

$$\phi_{tb} = \phi_p + \left(1 - \phi_p\right)\phi_u = \phi_p + \left(1 - \phi_p\right)\left(\phi_m + \left(1 - \phi_m\right)\phi_n\right), \tag{56}$$

The ratio between the mesoscopic and microscopic characteristic lengths is assumed to be in the order of $\varepsilon_0 = l_m / l_p = O\left(10^{-3}\right)$, which indicates a high permeability contrast condition and implies that the inner particle permeability does not affect the macroscopic flow[7,26]. This can be shown by comparing the respective velocities. The

ratio between the microscopic and mesoscopic velocities is in the order of [7,26]

$u_m / u_p = O\left(k_m / k_p\right) = O\left(\phi_m l_m^2 / \phi_p l_p^2\right) = O\left(10^{-6}\right)$ while that between the nanoscopic

and microscopic velocities depends on the dominant transport process at the

nanoscopic scale. If Knudsen diffusion dominates at the nanoscopic scale (i.e. in

nanopores in the order of tens of nanometers) this is given by

$u_n / u_m = O\left(D_g P_0^{-1} / k_m \eta^{-1}\right) = O\left(l_n l_{mean} / l_m^2 \left(1 + C_m \mathrm{Kn}\right)\right).$ Since $C_m \mathrm{Kn} < 5$ for

$l_m = O\left(l_{mean}\right)$ the estimation of the velocity ratio yields $u_n / u_m = O\left(10^{-5}\right)$. Adding

binary diffusion into the modelling does not significantly alter the order of magnitude

analysis since $D_{ij} = O\left(10^{-5}\right) \mathrm{m}^2/\mathrm{s}$ for most gases at normal conditions[2]. For smaller

nanopores (in the order of nanometers) in which condensate flow dominates, the

estimation of the fluid velocity ratio reads $u_n / u_m = O\left(l_n^2 \eta_l^{-1} / l_m^2 \eta^{-1}\right) = O\left(10^{-6}\right)$. Here it

has been assumed that the viscosity of the condensate is two orders of magnitude

larger than that of the gas[15]. To estimate the velocity ratio for the case where the

nanopores have a size in the order of that of gas molecules, an estimate of the

configurational diffusivity D_c is needed. For example, D_c of several gases in carbon

molecular sieve 5A was measured using chromatography in Ref.[33]. Its value for N2 at

20C can be calculated using the reported values of $D_{C\infty} = 1.5 \cdot 10^{-8} \mathrm{m}^2/\mathrm{s}$ and $E_c = 16.3$

kJ/mol as $D_c = 1.85 \cdot 10^{-11}$ m^2/s. Similarly, this parameter was measured in Ref.[34]

using a gravimetric technique for the same type of materials. Its value at 303K was

given by $D_c = 1.2 \cdot 10^{-10}$ m^2/s and $D_c = 6.5 \cdot 10^{-10}$ m^2/s for N2 and O2, respectively. In

Ref.[43] values of $D_{C\infty} = 1.98 \cdot 10^{-8}$ m^2/s and $E_c = 12.156$ kJ/mol were obtained for

diffusion of N2 in an activated carbon monolith by fitting experimental breakthrough

curves to a theoretical model. Using those values, the estimation of the

configurational diffusivity at 20C is given by $D_c = 1.35 \cdot 10^{-10}$ m²/s. In general, this parameter varies widely depending on the saturating fluid, the properties of the solid frame, and their interaction. Moreover, it can show remarkably different values depending on the measurement method used, as can be seen in figure 8 of Ref.[35] where D_c for the system propane-silicalite-1 measured with 9 different methods shows variations of about 4 orders of magnitude. As argued in Ref.[36], a value obtained from measurements using chromatography may be used for the practical purpose of estimating its order of magnitude. Therefore, the diffusivity D_c is considered to be in the order of 10^{-11}-10^{-10} m²/s and the velocity ratio $u_n / u_m = O\left(D_c P_0^{-1} / k_m \eta^{-1}\right)$ is then estimated as in the order of 10^{-7}- 10^{-6}.

These estimates confirm that, regardless of the dominant transport mechanism in the particles, the macroscopic flow is determined by the fluid flow at the mesoscopic (intergranular) scale and that the dynamic viscous permeability of the triple porosity material can be approximated as $k_{tb}(\omega) \approx k_p$ and is given by Eq. (43).

The dynamic bulk modulus of a triple porosity sorptive material is given by:

$$E_{tb}\left(\omega, \text{Kn}, b\right) = \left(\frac{1}{E_p} + \frac{\left(1 - \phi_p\right)}{E_u} F_d \right)^{-1}, \qquad (57)$$

Here the dynamic bulk modulus of the mesoscopic domain E_p is calculated by setting $\phi = \phi_p$ and $k' = k'_p$ in Eq. (37), and using Eq. (51) for k'_p. The function F_d that describes pressure diffusion effects is calculated by evaluating Eq. (55) at $z = \omega r_p \sqrt{\eta / j \omega k_u E_u}$, where the inner particle permeability is approximated as $k_u \approx k_m$ since the filtration velocity at the nanoscale is negligible compared to that of the microscopic fluid network and is calculated using Eq.(52).

The dynamic bulk modulus of the inner-particle scales E_u is calculated as:

$$E_u\left(\omega, \text{Kn}, b\right) = \left(\frac{1}{E_m} + \frac{\left(1-\phi_m\right)}{E_n} F_{nm}\right)^{-1}.$$ (58)

In this equation the dynamic bulk modulus of the microscopic domain E_m is calculated by setting $\phi = \phi_m$ and $k' = k'_m$ in Eq. (37) and noting that k'_m is calculated from Eq. (53). The dynamic bulk modulus of the nanoscopic scale is calculated using Eq. (39) for $\phi = \phi_n$. The function F_{nm} represents the inter-scale (nano-micro) mass diffusion (note that this is the same as G_q in Eq. 36 of Ref.[21] but for a bulk material instead of a single slit pore) and can be calculated using the scaling function[26] $F_{nm}\left(\omega\right) = 1 - j\omega_* B\left(\omega\right)/B_0$, where $B\left(\omega\right) = B_0(j\omega_* + \sqrt{1+j\omega_* M_b/2})^{-1}$, $\omega_* = \omega/\omega_{dnm}$, $\omega_{dnm} = \left(1-\phi_m\right)D_c/B_0$, and $M_b = 8B_0/\left(1-\phi_m\right)\Lambda_d^2$. For the inner particle geometry considered in this work (i.e. an array of cylindrical micropores whose walls are composed of an array of cylindrical nanopores) the parameters are given by[26] $B_0 = r_m^2\left(-\ln\phi_m - 3/2 + 2\phi_m - \phi_m^2/2\right)/4\phi_m$ and $\Lambda_d = r_m(1-\phi_m)/\phi_m$. Considering that $r_m = O(l_{mean})$ and D_c is in the order of 10^{-11}-10^{-10} m²/s, the characteristic frequency ω_{dnm} is between 2000 to 20000 rad/s. On the other hand, it is further noticed that the pressure diffusion characteristic frequency associated with F_d in Eq. (57), which is estimated as $\omega_d = O(P_0 l_m^2/\eta l_p^2)$, is of the same order or smaller than ω_{dnm} for the materials under study. This means that for frequencies much larger than ω_d the second term on the right-hand-side in Eq. (57) tends to zero and the contribution of the inner-particle physical phenomenon (i.e. sorption, diffusion, and rarefaction effects) becomes negligible, i.e. the overall bulk modulus at high frequencies is determined by that of the mesoscopic fluid network only. In practical terms, if the

condition $\omega_d \leq \omega_{dnm}$ is satisfied, one can consider that $F_{nm}(\omega) \approx 1$ or that the material is in "adsorption equilibrium control" following the denomination in Ref.[21] as the function F_d will approach to zero faster. The main advantage of this is that, in absence of measured values of D_c, this is not considered as another parameter to be adjusted. If the condition above is not satisfied, i.e. $\omega_d > \omega_{dnm}$, then the full model for $F_{nm}(\omega)$ should be taken into account.

Further considering isothermal sound propagation at the inner-particle scales (see Section II.A) leads to the following simplified expression for E_u:

$$E_{0u}(\omega \to 0, b) = \left(\frac{\phi_m}{P_0} + \frac{(1-\phi_m)\phi_n}{P_0} \left(1 + \Psi \rho_0^{-1} \rho_N \right) \right)^{-1}. \qquad (59)$$

Note that this assumption also implies that F_d in Eq. (57) should be evaluated at $z = r_p \omega \sqrt{\eta / j\omega k_{0u} E_{0u}}$, where[19] $k_{0u} = \phi_m r_m^2 (1 + 4\mathrm{Kn})/8$ is the static viscous permeability of the microscopic domain.

The macroscopic static bulk modulus is then calculated from Eqs. (57) and (59) as:

$$E_{tb}(\omega \to 0, b) = \frac{P_0}{\phi_{tb}} \frac{1}{\left(1 + \Theta \rho_0^{-1} \rho_N \Psi \right)}. \qquad (60)$$

where $\Theta = \phi_{tb}^{-1} (1 - \phi_p)(1 - \phi_m)\phi_n$.

The following conclusions can be made from Eq. (60). The static bulk modulus decreases when: i) the nanoporosity is increased, ii) the nanopore size is decreased (see Eq. (40)), and iii) the material is saturated with a fluid having heavier molecules or molecules with smaller surface area (see Eq. (40)).

The expressions for the characteristic impedance Z_c and wave number q_c of granular activated carbon; and those of normal incidence surface impedance Z_w, pressure

reflection coefficient R, and sound absorption coefficient α of a rigidly-backed layer of thickness d are now recalled[10]:

$$Z_c = \sqrt{\eta E_{tb} / j\omega k_{tb}} \text{ and } q_c = \omega\sqrt{\eta / j\omega k_{tb} E_{tb}} \qquad (61)$$

$$Z_w = -jZ_c \cot(q_c d), \ R = (Z_w - Z_0)/(Z_w + Z_0), \text{ and } \alpha = 1 - |R|^2, \qquad (62)$$

where $Z_0 = \rho_0 c_0$ is the characteristic impedance of air. These expressions are used to relate the effective permeability k_{tb} and effective bulk modulus E_{tb} with the quantities measured in the experiments.

In summary, a model for sound propagation in granular activated carbons has been proposed in this section. This model accounts for the existence of three scales of heterogeneities and depends on physical constants of the saturating fluid and seven parameters, namely the particle radius r_p, intergranular porosity (or mesoporosity) ϕ_p, micropore radius r_m, microporosity ϕ_m, nanopore radius r_n, nanoporosity ϕ_n, and the ratio between the adsorption and desorption constants, i.e. the Langmuir constant $b = k_a / k_d$. The next section proposes a methodology for the measurements or deduction of these parameter values from acoustical and/or non-acoustical measurements.

III. RESULTS AND DISCUSSIONS

A. Material characterization

Three activated carbon samples, denoted as sample A, B, and C, are investigated in this paper. Samples A and B are made out of coal and have very similar intergranular characteristics but different intragranular ones. Sample C is made out of coconut shell and its intragranular characteristics are very similar to those of sample A but their intergranular ones differ. The model parameters for these samples are shown in

Acoustics of granular activated carbon

TABLE I. It is explained throughout this section how these parameters have been measured or calculated.

	ϕ_p	r_p [mm]	ϕ_m	r_m [μm]	ϕ_n	r_n [nm]	$b \times 10^6$ [1/Pa]	ϕ_{tb}
A	0.2997	0.7363	0.7064	0.4131	0.2593	0.3303	3.4696	0.8477
B	0.3083	0.7536	0.5571	0.2054	0.1602	0.2386	3.9565	0.7427
C	0.332	0.3062	0.6639	0.0958	0.2791	0.4060	8.5242	0.8381

TABLE I. Model parameters of granular activated carbon samples.

1. Equivalent particle radius

An equivalent particle radius r_p of the granular activated carbon samples has been measured using optical granulometry following the procedure detailed in Ref.[6,7]. The complementary cumulative equivalent particle radius distribution for the three activated carbon samples is shown in Figure 4. For example, 75% of the particles of the sample A have an equivalent particle radius larger than 0.639 mm. The equivalent particle radius distribution for the sample A and B follows a log-normal distribution[37]

$$f\left(t|\mu,\theta\right)=\left(1/t\theta\sqrt{2\pi}\right)\exp\left(-\left(\ln\left(t\right)-\mu\right)^2/2\theta^2\right)$$ with parameters $\mu=-7.2513$ and $\theta=0.2741$, and $\mu=-7.2129$ and $\theta=0.2112$, respectively; while that for the sample C follows a Weibull distribution[37] $f\left(t|\mu,\theta\right)=\left(\theta/\mu\right)\left(t/\mu\right)^{\theta-1}\exp\left(\left(t/\mu\right)^{\theta}\right)$ with parameters $\mu=3.382\cdot10^{-4}$ and $\theta=3.9126$. Therefore, the mean value and standard deviation (in parenthesis) of the equivalent particle radius distribution for the samples A, B, and C are 0.7363 (0.2056) mm, 0.7535 (0.1609) mm, and 0.3062

(0.0876) mm respectively. The equivalent particle radius r_p is set to the mean value of the equivalent particle radius distribution, as shown in TABLE I.
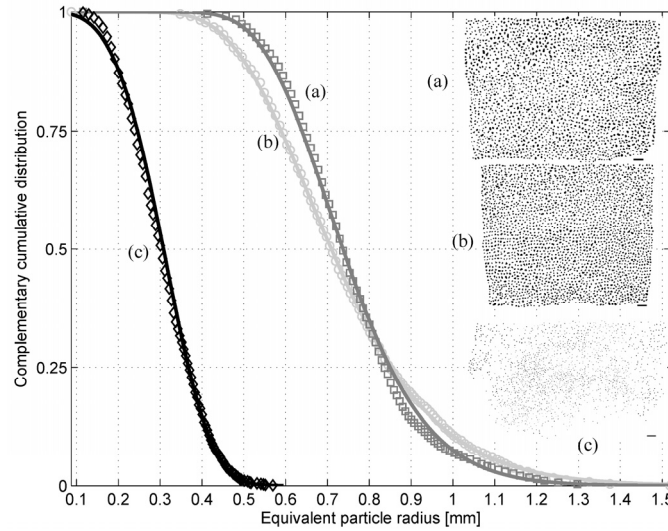

Figure 4: Complementary cumulative equivalent particle radius of granular activated carbon samples A (a), B (b), and C (c). Markers - data. Lines – fitted distributions. The inset plots correspond to the processed images for samples A (a), B (b), and C (c). The black rectangle at the bottom-right of these images represents 10 mm. The number of particles considered for the samples A, B, and C are 2208, 2439, and 1880 respectively.

2. Flow resistivity measurements and mesoporosity estimation

Since the granular activated carbons exhibit high permeability contrast, which implies that the overall permeability can be approximated by that of the mesoscopic fluid flow network, measurements of flow resistivity can be used to estimate the mesoporosity[7]. The flow resistivity has been measured by following the standard procedure detailed in Ref.[38]. Figure 5 shows the flow resistivity as a function of the flow rate for the three granular activated carbon samples. For the samples A and B measurements on layers 2-cm and 4-cm thick have been conducted in an attempt to estimate the variability of the flow resistivity with respect to both the packing condition and the

layer thickness. TABLE II shows the static flow resistivity values as well the estimated values of the mesoporosity. This has been calculated by inverting the theoretical expression for flow resistivity calculated as $\sigma_{0p} = \eta / k_{0p}$ with the static viscous permeability k_{0p} being given by Eq.(50). The equivalent particle radius measured previously has been also used in the calculation of the mesoporosity. The observed variability in flow resistivity is 6.14% for the sample A and 6.85% for the sample B. This corresponds to an average variability in mesoporosity of 1.77% and 1.62% respectively. The flow resistivity and the mesoporosity can be considered as thickness independent and both are not significantly affected by the activated carbon packing conditions. This justifies having taken only one flow resistivity measurement for the sample C. The mesoporosity presented in TABLE I corresponds to the average value of mesoporosity shown in TABLE II.
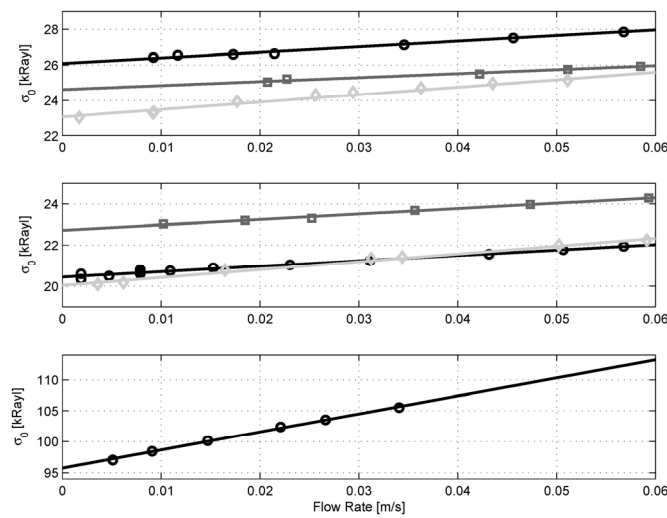

Figure 5: Flow resistivity as a function of the flow rate for the granular activated carbon sample A (top), B (middle), and C (bottom). Diamonds - measurements for a 4-cm layer. Circles and Squares - measurements for 2-cm layers of different samples but the same material. Lines are fitted straight lines.

	Flow resistivity [kRayl]			Mesoporosity ϕ_p		
Measurement	A	B	C	A	B	C
(a) d = 4 cm	23.0667	20.0410	--	0.305	0.312	--
(b) d = 2 cm	24.6232	20.4436	--	0.299	0.302	--
(c) d = 2 cm	26.0870	22.7196	95.7414	0.295	0.311	0.332
Average	24.5923 (1.5104)	21.068 (1.444)	95.7414	0.2997 (0.005)	0.3083 (0.005)	0.332

TABLE II. Measured flow resistivity of the activated carbon samples and their mesoporosity estimations. Standard deviation values are shown in brackets.

3. Overall, micro- and nano porosity measurements

The overall porosity has been calculated as $\phi_{tb} = 1 - \rho_b / \rho_c$ using measurements of the bulk density of the samples ρ_b and the density of the solid frame, which is assumed to be that of carbon black, i.e. $\rho_c = 2.2 \, \text{g/cm}^3$. The bulk density ρ_b of the samples A, B, and C is 0.335 g/cm^3, 0.566 g/cm^3, and 0.356 g/cm^3 respectively. The nanoscopic porosity has been calculated as $\phi_n = \rho_b V_n$ using the bulk density of the materials and the known nanopore (0-2 nm) volume V_n (or micropore volume as defined in Ref. [32]). The nanopore volume measured using a standard isotherm measurement technique, i.e. Nitrogen @ 77 K, and the Dubinin-Radushkevich method[1,2,39] has been provided by the sample manufacturer and is equal to 0.774 cm^3/g, 0.283 cm^3/g, and 0.784 cm^3/g for the samples A, B, and C respectively. The microporosity has been deduced from Eq. (56) as $\phi_m = \left(\left(\phi_{tb} - \phi_p \right) - \phi_n \left(1 - \phi_p \right) \right) / \left(1 - \phi_p \right)\left(1 - \phi_n \right)$. All porosity values are shown in TABLE I.

Acoustics of granular activated carbon   33

4. Bulk modulus measurements and estimation of Langmuir constant and micro- and nanopore radii

The bulk modulus for the granular activated carbon samples has been measured using the two-thickness method[40] and is shown in Figure 6. The anomalous behavior of the bulk modulus of activated carbon, i.e. its static value less than unity, is clearly observed. The measured normalized static bulk modulus, i.e $E_{tb}^* = \mathrm{Re}\left(E_{tb}\left(\omega \to 0\right)\right)/P_0$, has been estimated by extrapolating the real part of the dynamic bulk modulus to zero frequency. This corresponds to 0.4277, 0.5026, and 0.3542 for the samples A, B, and C respectively. The inset plot shows the measurement of the bulk modulus for an array of non-porous particles[7] (lead shots) with porosity $\phi_p = 0.39$ and mean particle radius of $r_p = 0.55\,\mathrm{mm}$ (see section III.A in Ref.[7] for more details about this material and its characterization). It is clear that the normalised bulk modulus of the collection of lead shots tends to the classical value of the inverse of porosity at low frequencies.
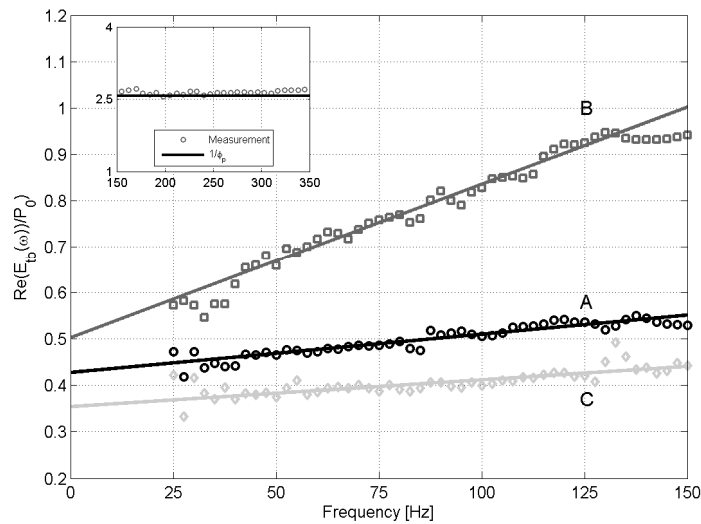

Figure 6: Real part of the dynamic bulk modulus of granular activated carbon samples A, B, and C. Markers – measured data. Lines – fitted straight lines. The inset plot shows the same parameter but for an array of non-porous particles (lead shots).

The micropore and nanopore radii, i.e. r_m and r_n, have been calculated through a best

fitting routine using the differential evolution algorithm[41]. This routine minimises the

square of the absolute difference between the predicted and measured characteristic

impedance. As part of this routine the Langmuir constant b is calculated so as to

match the predicted normalised static bulk modulus with its measured value using

$2b = P_0^{-1}\Psi^{-1}\left(1 - 2\Psi - \sqrt{1 - 4\Psi}\right)$ where the dimensionless parameter Ψ is estimated

as $\Psi = \rho_0 \rho_N^{-1} \Theta^{-1}((E_{tb}^* \phi_{tb})^{-1} - 1)$. The values of r_m, r_n, and b are shown in TABLE I.

For the three samples the values for r_m and r_n are in the order of those commonly

found in activated carbon[1,2]. It must be emphasised that these values should not be

considered as realistic pore radii, instead they represent the effective pore sizes. This

is because the complicated inner geometry of a highly heterogeneous activated carbon

has been approximated in the model by ordered arrays of cylindrical monodisperse

micro and nanopores. However, r_m and r_n values and the measured equivalent

particle radius confirm the assumptions of high-permeability contrast between the

meso and micro scales, respectively.

Furthermore, the values obtained for r_m and r_n also validate the assumption $F_{nm} \approx 1$

for the scaling function in Eq. (58) which relies on the condition $\omega_d \leq \omega_{dnm}$.

Considering that $\omega_d = (1 - \phi_p)P_0 k_m / \phi_m \eta D_0$, where $D_0 = (1 - \phi_p)r_p^2 / 15$, one can

deduce that the condition for the characteristic frequencies is satisfied for

configurational diffusivity values $D_c \geq (1 - \phi_p)P_0 k_m B_0 / (1 - \phi_m)\phi_m \eta D_0$. From this

inequality, the minimum configurational diffusivity values for the condition

$\omega_d \leq \omega_{dnm}$ to be satisfied are given by $1.18 \cdot 10^{-11}$, $3.28 \cdot 10^{-12}$, and $6.61 \cdot 10^{-13}$ m^2/s for

the samples A, B, and C respectively. Since D_c is in the order of 10^{-11}-10^{-10} m^2/s for the materials under study (see Section II.C), it is then concluded that the condition $\omega_d \leq \omega_{dnm}$ is satisfied and the simplifying assumption $F_{nm} \approx 1$ is thereby validated.

Since air is mostly composed of nitrogen the obtained values for the Langmuir constant, which are in the order of 10^{-6} 1/Pa, are compared to those reported in literature for nitrogen adsorption on to activated carbon. Isotherm measurements in Ref.[42] were taken at different temperatures (ranging from 30C to 60C) on a granular activated carbon sample with particle size 0.85-1.70 mm and a BET surface area of 1200 m^{2}g^{-1}, which is a material comparable to sample A in this paper. The Langmuir constant was calculated as[42] $b = b_0 \exp\left(-\Delta H / R_g T\right)$, where the pre-exponential value b_0 and the average isosteric heat of adsorption ΔH were obtained by fitting the measured data to the Langmuir model. The reported values for these parameters are[42] $b_0 = 1.2089 \cdot 10^{-10}$ 1/Pa and $\Delta H = -24.12$ kJ.mol^{-1}, which at normal conditions results in $b = 2.3995 \cdot 10^{-6}$ 1/Pa. In Ref.[43] measurements on an activated carbon sample in monolithic form were presented. The reported parameters are[43] $b_0 = 1.76 \cdot 10^{-9}$ 1/Pa and $\Delta H = -17.082$ kJ.mol^{-1}, which yields at normal conditions $b = 1.9462 \cdot 10^{-6}$ 1/Pa. In Ref.[44] the Langmuir-Freundlich model was used to fit the measured data for a PCB-type activated carbon with average grain size of 0.115 mm and BET surface area of 1150-1250 m^{2}g^{-1} (comparable to sample C in this paper). At normal pressure and temperature an effective Langmuir constant of $b = 2.9441 \cdot 10^{-6}$ 1/Pa can be deduced. It is pertinent to note that the Langmuir constant for oxygen is of the same order of magnitude. Hence the values obtained for the Langmuir constant in the present paper correlate well with those found in literature.

B. Comparison with data and discussions

Measurements of normal incidence surface impedance and sound absorption coefficient of granular activated carbons were performed using a vertically-installed B&K 4206 impedance tube. The two-microphone method described in the standard ISO 10534-2[45] was followed. Measured data for rigidly-backed 2-cm layers of different granular activated carbon samples are compared with the values predicted by the model in Figure 7. Note that the predictions obtained by assuming that sorption effects are negligible are also plotted for comparison. A good agreement between the data and the model predictions is observed. It is worth highlighting that the imaginary part of the surface impedance at low frequencies tends to $\mathrm{Im}\{Z_w(\omega \to 0)\} = -E_{tb}(\omega \to 0)/\omega d$. From this equation and Eq. (60) one can conclude that the smaller than usual values of the surface impedance imaginary part at low frequencies are a direct consequence of its anomalous bulk modulus; and hence attributed to sorption effects. As follows from Eq. (61) and (62) the layer thickness in the denominator of the low-frequency approximation of the surface impedance is multiplied by a factor of $\phi_{tb}\left(1 + \Theta \rho_0^{-1} \rho_N \Psi\right)$ instead of just the overall porosity ϕ_{tb}. This means that a layer of granular activated carbon tends to behave, acoustically, as if it were thicker than it physical is, which makes this material attractive for acoustical applications where space is constrained.

Figure 8 shows the measured and predicted normal incidence sound absorption coefficient of rigidly-backed 3-cm layers of different granular activated carbon samples. A good agreement is observed between measurements and predictions. The slight disagreement between the data and the predictions for the sample C around 300 Hz is due to the vibration of the grains[6], which is not accounted for in the model.

Sample A provides a much larger low-frequency sound absorption coefficient than sample B. It is worth reminding that the samples A and B have nearly identical mesoscopic properties (mesoporosity, particle radius, and flow resistivity) but different inner-particle characteristics (see TABLE I). These differences account for those in absorption coefficients at low frequencies. On the other hand, samples A and C have similar inner-particle characteristics but different mesoscopic ones. The particle size strongly affects the flow resistivity value and the larger it is the lower is the high frequency sound absorption coefficient. The inset plot shows a good agreement between the predictions of the model for an array of non-porous particles (lead shots) and the measured values. To further highlight the absorptive properties of granular activated carbon, the predictions of the model for an array of non-porous particles with the same mesoscopic parameters (particle radius and mesoporosity) as those of sample A, B, and C are also plotted in the main figure. As previously shown in Ref.[7], the sound absorption coefficient of an array of non-porous particles is remarkably different than that of granular activated carbon. It is worth mentioning that because of the nearly identical mesoscopic characteristics of the samples A and B the model would predict a nearly the same sound absorption coefficient, which is clearly not the case.

The sound absorption coefficient of 4-cm thick rigidly-backed layers of activated carbon is shown in Figure 9. The proposed model is able of capturing the general sound absorptive trend at high frequencies as well. Some discrepancies found in this frequency range are likely to be due the underestimation of the material tortuosity by the analytical model[6].
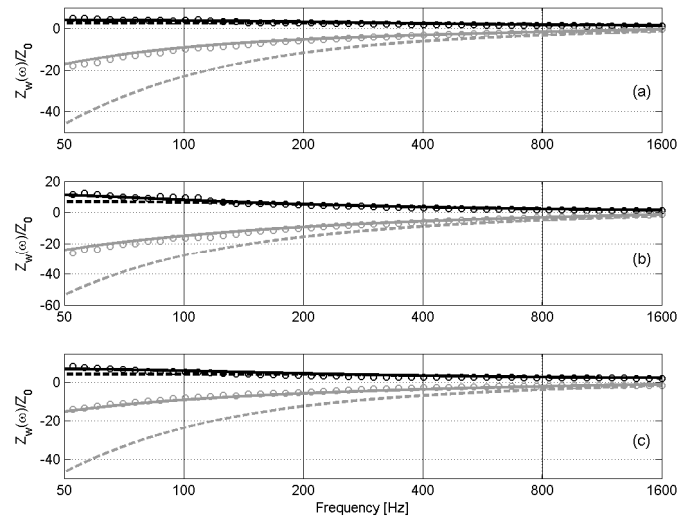
Figure 7: Normalized surface impedance of a rigidly-backed 2-cm layer of granular activated carbon samples A (a), B (b), and C (c). Markers - measurements. Continuous lines - predictions of the model proposed in this work. Dashed lines - predictions obtained assuming negligible sorption effects. Black - real part. Grey - imaginary part.
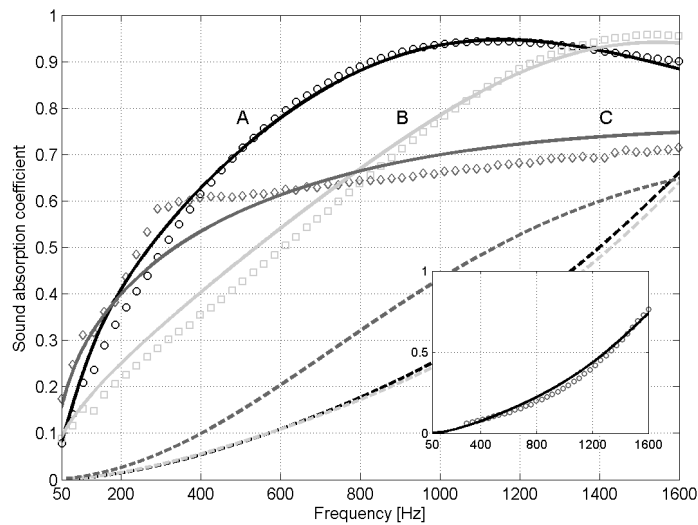

Figure 8: Normal incidence sound absorption coefficient of a rigidly-backed 3-cm layer of granular activated carbon sample A, B and C. Markers - measurements. Lines - predictions. Dashed lines - predictions for a packing of non-porous particles with the same mesoscopic properties as those of samples A, B, and C. The inset plot shows the predictions (line) of the model for an array of non-porous lead shots and the measured values (circles).
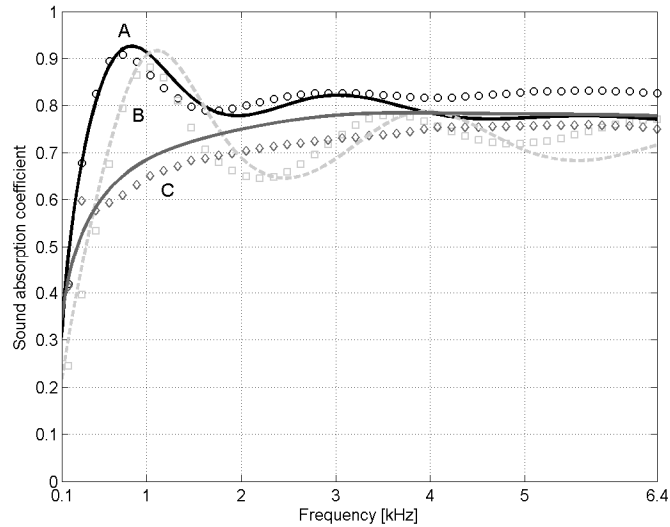
Figure 9: Normal incidence sound absorption coefficient (up to 6.4 kHz) of a rigidly-backed 4-cm layer of granular activated carbon sample A, B and C. Markers - measurements. Lines - predictions.

Finally, the sensitivity of sound absorption coefficient to the values of Langmuir constant and nanopore and micropore radii is illustrated by Figure 10. The particle radius and porosities of the sample A, as well as the layer thickness (d=3cm), have been kept constant in this analysis. The grey area in the main plot shows where the predicted values for sound absorption coefficient for different values of the Langmuir constant and nanopore radius fall. These have been varied from 10^{-8} to 10^{-5} 1/Pa and from the size of an air molecule to 1 nm, respectively (note that the micropore radius has been kept constant). As previously discussed, by minimising the static bulk modulus an increase of the absolute value of the imaginary part of the surface impedance is achieved. In turn, this allows the material to acoustically behave as if it were thicker than it physically is. Therefore, it is not surprising that the limiting upper value of the sound absorption coefficient corresponds to the largest Langmuir constant and the smallest nanopore radius. The lower limiting value corresponds to the smallest Langmuir constant and largest nanopore radius within the range

Acoustics of granular activated carbon   40

considered, and approaches both that of a non-sorptive triple porosity material and that of a double porosity non-sorptive material. A collection of non-porous particles provides much lower sound absorption coefficient values. The inset plot shows the influence of the micropore radius. This has been varied so that the condition $\omega_d \leq \omega_{dnm}$ is satisfied, i.e. $r_m \in [0.06, 0.74]$ μm for the sample A (the other parameters are kept constant). An increase in sound absorption coefficient is observed as the micropore radius increases. This is a direct consequence of the dissipation of sound energy caused by pressure diffusion effects around the characteristic frequency ω_d. The influence of the other parameters, e.g. porosities and particle radius, has been investigated in Ref.[6].
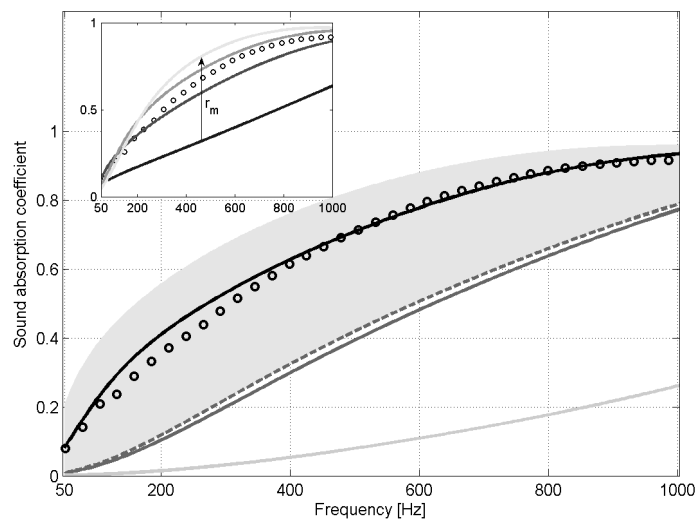

Figure 10: Sensitivity of sound absorption coefficient α to the Langmuir constant and nanopore and micropore radii. Main plot: Predictions of the model for i) a triple porosity sorptive (black line) and non-sorptive (dahsed grey line) material, ii) a double porosity non-sorptive material ($\phi_n = 0$, continuous grey line), and iii) a packing of non-porous particles ($\phi_n = \phi_m = 0$, continuous light grey line). The grey area shows α for different combinations of Langmuir constant and nanopore radius values (see the text for more details). Inset plot: Influence of the micropore radius. Measured values are shown with markers.

IV. CONCLUSIONS

A model for sound propagation in granular activated carbon has been developed which takes into account three scales of heterogeneities (i.e. meso, micro, and nano scales) and physical processes specific to small pores, e.g. rarefaction at the microscopic scale and sorption at the nanoscopic scale. The model is capable of predicting both the anomalous behaviour of the bulk modulus and the unusually large low frequency sound absorption by granular activated carbons. The latter is shown to be in direct correlation with the amount of nanometre size pores and hence is attributed to sorption processes.

In general, the dissipation of sound energy in granular activated carbon is caused by viscosity and heat conduction effects at the mesoscopic scale (intergranular voids), pressure diffusion between the mesoscopic and inner-particle scales (affected by rarefaction effects), and the effect the sorption processes at the nanoscopic scale. The macroscopic bulk modulus and pressure diffusion characteristics of the multi-scale material are modified in response to a local increase of density in very small pores caused by the adsorbed molecules.

A methodology for the acoustic characterisation of granular activated carbon that included different techniques, e.g. optical granulometry and flow resistivity, isotherm, porosity, and acoustic measurements, and a best fitting routine, was also introduced. Using this methodology the obtained model parameters were found physically plausible, similar to those commonly encountered in granular activated carbon, and provided accurate predictions of the acoustical properties of granular activated carbon.

Despite the good agreement between the measurements and the predictions, it has to be reminded that the Langmuir constant was not measured directly and two of the

model parameters (nanopore radius r_n and micropore radius r_m) were adjusted. This suggests that model as it stands may only be applicable to materials similar to granular activated carbon saturated by air at normal conditions. A complete validation of the model, and consequently its generalization to a wider class of granular adsorbents, would require taking direct measurements of all the model parameters (including the configurational diffusivity) and/or measurements of the acoustical properties of granular activated carbon at different temperature, pressure, and/or saturating gas conditions; as this would allow varying the sorption behavior of the material. For example, saturating the material with helium would provide an interesting way of suppressing the sorption effect.

Moreover, rarefaction and sorption processes are not the only physical processes likely to be influencing sound propagation in materials with very small pores. For example, activated diffusion, surface diffusion, film condensate flow, capillary condensate flow, molecular diffusion, and Knudsen diffusion have been reported to significantly influence the isothermal mass transport in activated carbon[2,14,15,16,17,36,46,47,48]. Some of these processes have been considered in the model but a detailed investigation of their influence on sound interaction with multiscale porous materials is an interesting topic for future research that might lead to their more effective exploitation in acoustics.

Acknowledgements

References

[1] H. Marsh and F. Rodriguez-Reinoso, *Activated Carbon*, (Elsevier Science & Technology Books, Oxford, 2006). p. 1-554.

[2] D. D. Do, *Adsorption analysis: Equilibria and Kinetics*, (Imperial College Press, London, 1998). p. 1-892.

[3] J.R. Wright, "The virtual loudspeaker cabinet," J. Audio Eng. Soc. **51**(4), 244–247 (2003).

[4] T. J. Mellow, O. Umnova, K. Drossos, K. Holland, A. Flewitt, and L. Karkkainen, "On the adsorption-desorption relaxation time of carbon in very narrow ducts," in Proceedings of Acoustics 08, CD-ROM 01, p. 795–800, Paris, France, 2008.

[5] F. Bechwati, M. Avis, D. Bull, T. J. Cox, J. Hargreaves, D. Moser, D. Ross, O. Umnova, and R. Venegas, "Low frequency sound propagation in activated carbon," J. Acoust. Soc. Am. **132**(1), 239-248 (2012).

[6] R. Venegas, "Microstructure influence on acoustical properties of multiscale porous materials," Ph.D. dissertation, University of Salford, U.K., 2011.

[7] R. Venegas and O. Umnova, "Acoustic properties of double porosity granular materials," J. Acoust. Soc. Am. **130**(5), 2765–2776 (2011).

[8] F. Bechwati, T. J. Cox, and O. Umnova, "New semi-empirical model for sound propagation in adsorbing microporous solid (activated carbon)," Proceedings of 19th International Congress on Acoustics, PHY-03-012, Madrid 2-7 September (2007).

[9] C. Shen, *Rarefied Gas Dynamics, Fundamentals, Simulations and Micro Flows*, (Springer-Verlag, Berlin, 2005). p. 1-406.

[10] J. F. Allard and N. Atalla, *Propagation of Sound in Porous Media: Modeling Sound Absorbing Materials* (John Wiley & Sons, New York, 2009), Chaps. 2–5.

[11] J. L. Auriault, L. Borne, and R. Chambon, "Dynamics of porous saturated media, checking of the generalized law of Darcy," J. Acoust. Soc. Am. **77**(5), 1641–1650 (1985).

[12] J. L. Auriault, C. Boutin, and C. Geindreau, *Homogenization of Coupled Phenomena in Heterogenous Media* (John Wiley & Sons, London, 2009). p. 1-472.

[13] J.C. Maxwell, "On stresses in rarefied gases arising from inequalities of temperature," Phil. Trans. R. Soc. Part 1 **170**, 231–56 (1879).

[14] D. D. Do and K.Wang, "A new model for the description of adsorption kinetics in heterogeneous activated carbon," Carbon **36** (10), 1539–1554 (1998).

[15] H. D. Do and D.D. Do, "A new diffusion and flow theory for activated carbon from low pressure to capillary condensation range," Chem. Eng. J. **84**, 295–308 (2001).

[16] S. W. Rutherford and D. D. Do, "Knudsen, slip, and viscous permeation in a carbonaceous pellet," Ind. Eng. Chem. Res. **38**, 565-570 (1999).

[17] Suzuki, M, *Adsorption Engineering*, (Kodansha Ltd. & Elsevier Science, Tokyo, 1989). p. 63-93.

[18] M. Von Smoluchowski, "Ueber Wärmeleitung in verdünnten Gasen," Ann. Phys. Chem. **64**, 101–30 (1898).

[19] V. F. Kozlov, A. V. Fedorov, and N. D. Malmuth, "Acoustic properties of rarefied gases inside pores of simple geometries," J. Acoust. Soc. Am. **117**, 3402–3411 (2005).

[20] O. Umnova, D. Tsiklauri, and R. Venegas, "Effect of boundary slip on the acoustical properties of microfibrous materials," J. Acoust. Soc. Am. **126** (4), 1850-1861 (2009).

[21] M. Nori and S. Brandani, "A model for sound propagation between two adsorbing microporous plates," J. Acoust. Soc. Am. **135**(5), 2634-2645 (2014).

[22] E. Sanchez-Palencia, *Nonhomogeneous Media and Vibration Theory*, Lecture Notes in Physics, edited by J. Ehlers, K. Hepp, R. Kippenhahn, and J. Zittartz (Springer-Verlag, Berlin, 1980). p. 1-398.

[23] C. Cercignani, *Slow Rarefied Flows*, (Birkhäuser Verlag, Basel, 2006). p. 1-166.

[24] I. Langmuir, "The constitution and fundamental properties of solids and liquids," J. Am. Chem. Soc. **38** (11), 2221–2295 (1916).

[25] C. Boutin, P. Royer, and J. L. Auriault, "Acoustic absorption of porous surfacing with dual porosity," Int. J. Solids Struct. **35**, 4709–4737 (1998).

[26] X. Olny and C. Boutin, "Acoustic wave propagation in double porosity media," J. Acoust. Soc. Am **114**(1), 73–89 (2003).

[27] J. Chastanet, P.Royer, and J.-L.Auriault, "Acoustics with wall-slip flow of gas saturated porous media," Mech. Res. Commun. **31**, 277-286 (2004).

[28] L.-Z. Zhang, *Conjugate Heat and Mass Transfer in Heat Mass Exchanger Ducts*, (Elsevier, Oxford, 2014). p.36.

[29] J. Chastanet, P. Royer and J.-L. Auriault, "Flow of low pressure gas through dual-porosity media," Transp. Porous Media **66** (3), 457-479 (2007).

[30] C. Boutin and C. Geindreau, "Estimates and bounds of dynamic permeability of granular media," J. Acoust. Soc. Am. **124**(6), 3576–3593 (2008).

[31] C. Boutin and C. Geindreau, "Periodic homogenization and consistent estimates of transport parameters through sphere and polyhedron packings in the whole porosity range," Phys. Rev. E **82**, 036313 (2010).

[32] K.S.W. Sing, D.H. Everett, R.A.W. Haul, L. Moscon, R.A. Pierotti, J. Rouguerol, and T. Siemieniewska,"Reporting Physisorption Data for Gas/Solid Systems with Special Reference to the Determination of Surface Area and Porosity (Recommendations 1984)," Pure Appl Chem. **57** (4), 603–619 (1985).

[33] K. Chihara, M. Sukuzi, and K. Kawazoe, "Adsorption rate on molecular sieving carbon by chromatography," AIChE Journal, **24** (2), 237-245 (1978).

[34] Y. H. Ma, W. Sun, M. Bhandarkar, J. Wang, and G. W. Miller, "Adsorption and diffusion of nitrogen, oxygen, argon, and methane in molecular sieve carbon at elevated pressures," Separ. Technol., **1**, 90-98 (1991).

[35] T.A. Nijhuis, L.J.P. van den Broeke, M.J.G. Linders, J.M. van de Graaf, F. Kapteijn, M. Makkee, and J.A. Moulijn, "Measurement and modeling of the transient adsorption, desorption and diffusion processes in microporous materials," Chem. Eng. Sci., **54**, 4423-4436 (1999).

[36] R. T. Yang, *Gas separation by adsorption processes*, (Butterworth Publishers, Stoeham, 1987). p. 121.

[37] M. Evans, N. Hastings, and B. Peacock, *Statistical distributions*, 3rd edition, (John Wiley & Sons, New York, 2000). p. 1-221.

[38] BS EN 29053:1993, "Acoustics. Materials for acoustical applications. Determination of airflow resistance," 1993.

[39] DIN 66135-3, "Particle characterization - Micropore analysis by gas adsorption - Part 3: Determination of the micropore volume according to Dubinin and Radushkevich," 2001.

[40] C. D. Smith and T.L. Parrott, "Comparison of three methods for measuring acoustic properties of bulk materials," J. Acoust. Soc. Am. **74**(5), 1577-1582 (1983).

[41] K. Price, R. Storn and J. Lampinen, *Differential Evolution: A Practical Approach to Global Optimization*, (Springer-Verlag, Berlin, 2005). p. 1-560. See also http://www.icsi.berkeley.edu/~storn/code.html. Last checked on 26th May 2016.

[42] S. A. Al-Muhtaseb, F. A. A. Al-Rub, and M. Al Zarooni, "Adsorption equilibria of nitrogen, methane, and ethane on BDH-activated carbon," J. Chem. Eng. Data **52**, 60-65 (2007).

[43] R. P. Ribeiro, T. P. Sauer, F. V. Lopes, R. F. Moreira, C. A. Grande and A. E. Rodrigues, "Adsorption of CO2, CH4, and N2 in activated carbon honeycomb monolith," J. Chem. Eng. Data **53**, 2311–2317 (2008).

[44] B.-U. Choi, D.-K. Choi, Y.-W. Lee, and B.-K. Lee, "Adsorption equilibria of methane, ethane, ethylene, nitrogen, and hydrogen onto activated carbon," J. Chem. Eng. Data **48**, 603-607 (2003).

[45] ISO 10534-2:2001, "Acoustics—Determination of sound absorption coefficient and impedance in impedance tubes—Part 2: Transfer-function method, 2001.

[46] E. A. Flood, R.H. Tomlinson, and A.E. Leger, "The flow of fluids through activated carbon rods, I, II and III," Can. J. Chem. **30** (5), 348-410 (1952).

[47] R. F. Bartholemew and E. A. Flood, "The flow of gases through microporous carbon," Can. J. Chem. **43** (5), 1986-1972 (1965).

[48] J.-S. Bae and D. D. Do, "Surface diffusion of strongly adsorbing vapors in activated carbon by a differential permeation method," Chem. Eng. Sci. **58**, 4403-4415 (2003).

TABLE I. Model parameters of granular activated carbon samples.

	ϕ_p	r_p [mm]	ϕ_m	r_m [μm]	ϕ_n	r_n [nm]	$b \times 10^6$ [1/Pa]	ϕ_{tb}
A	0.2997	0.7363	0.7064	0.4131	0.2593	0.3303	3.4696	0.8477
B	0.3083	0.7536	0.5571	0.2054	0.1602	0.2386	3.9565	0.7427
C	0.332	0.3062	0.6639	0.0958	0.2791	0.4060	8.5242	0.8381

TABLE II. Measured flow resistivity of the activated carbon samples and their mesoporosity estimation. Standard deviation values are shown in brackets.

	Flow resistivity [kRayl]			Mesoporosity ϕ_p		
Measurement	A	B	C	A	B	C
(a) d = 4 cm	23.0667	20.0410	--	0.305	0.312	--
(b) d = 2 cm	24.6232	20.4436	--	0.299	0.302	--
(c) d = 2 cm	26.0870	22.7196	95.7414	0.295	0.311	0.332
Average	24.5923 (1.5104)	21.068 (1.444)	95.7414	0.2997 (0.005)	0.3083 (0.005)	0.332

FIGURE CAPTIONS

Figure 1: Diagram of the scales of a single porosity material supporting rarefaction and sorption effects (adapted from Ref.[12])

Figure 2: Diagram of the scales of a double porosity material (adapted from Ref.[26])

Figure 3: Diagram of the scales of a triple porosity sorptive material

Figure 4: Complementary cumulative equivalent particle radius of granular activated carbon samples A (a), B (b), and C (c). Markers - data. Lines – fitted distributions. The inset plots correspond to the processed images for samples A (a), B (b), and C (c). The black rectangle at the bottom-right of these images represents 10 mm. The number of particles considered for the samples A, B, and C are 2208, 2439, and 1880 respectively.

Figure 5: Flow resistivity as a function of the flow rate for the granular activated carbon sample A (top), B (middle), and C (bottom). Diamonds - measurements for a 4-cm layer. Circles and Squares - measurements for 2-cm layers of different samples but the same material. Lines are fitted straight lines.

Figure 6: Real part of the dynamic bulk modulus of granular activated carbon samples A, B, and C. Markers – measured data. Lines – fitted straight lines. The inset plot shows the same parameter but for an array of non-porous particles (lead shots).

Figure 7: Normalized surface impedance of a rigidly-backed 2-cm layer of granular activated carbon samples A (a), B (b), and C (c). Markers - measurements. Continuous lines - predictions of the model proposed in this work. Dashed lines - predictions obtained assuming negligible sorption effects. Black - real part. Grey - imaginary part.

Figure 8: Normal incidence sound absorption coefficient of a rigidly-backed 3-cm layer of granular activated carbon sample A, B and C. Markers - measurements. Lines - predictions. Dashed lines -

predictions for a packing of non-porous particles with the same mesoscopic properties as those of samples A, B, and C. The inset plot shows the predictions (line) of the model for an array of non-porous lead shots and the measured values (circles).

Figure 9: Normal incidence sound absorption coefficient (up to 6.4 kHz) of a rigidly-backed 4-cm layer of granular activated carbon sample A, B and C. Markers - measurements. Lines - predictions.

Figure 10: Sensitivity of sound absorption coefficient α to the Langmuir constant and nanopore and micropore radii. Main plot: Predictions of the model for i) a triple porosity sorptive (black line) and non-sorptive (dahsed grey line) material, ii) a double porosity non-sorptive material ($\phi_n = 0$, continuous grey line), and iii) a packing of non-porous particles ($\phi_n = \phi_m = 0$, continuous light grey line). The grey area shows α for different combinations of Langmuir constant and nanopore radius values (see the text for more details). Inset plot: Influence of the micropore radius. Measured values are shown with markers.

Macroscopic scale

Microscopic scale $\boldsymbol{\Omega}$

L

l

$\mathbf{t}_1$

$\mathbf{n}$

Γ_s

$\boldsymbol{\Omega}_f$

Pores

Macroscopic scale

Mesoscopic scale
REVp $\quad \Omega_p$

L

Γ_{sp}

Micro-porous
domain

Ω_{sp}

l_p

Pores $\quad \Omega_{fp}$

Γ_{fm}

Γ_{fp}

$\mathbf{t}_1$

Solid

$\mathbf{n}$

l_m

Micro-pores $\quad \Omega_{fm}$

Γ_{sm}

Microscopic scale
REVm $\quad \Omega_m$

Macroscopic scale

L

Mesoscopic scale
REVp Ω_p

Γ_{sp}

Microporous
domain
Ω_{sp}

Ω_{fp}

l_p

Pores

Γ_{fp}

Nanoscopic scale Ω_n

REVn

l_n

$\mathbf{t}_1$

$\mathbf{n}$

Γ_{sn}

Ω_{fn}

Solid

Γ_{fn}

Nanopores

Microscopic scale
REVm Ω_m

Nanoporous
domain
Ω_{sm}

$\mathbf{t}_1$

$\mathbf{n}$

Γ_{sm}

Ω_{fm}

l_m

Γ_{fm}

Micropores